Beamforming with a circular microphone array for localization of environmental noise sources

Article *in* The Journal of the Acoustical Society of America · December 2010

DOI: 10.1121/1.3500669 · Source: PubMed

Beamforming with a circular microphone array for localization of environmental noise sources[a)]

Elisabet Tiana-Roig,[b)] Finn Jacobsen, and Efrén Fernández Grande
Acoustic Technology, Department of Electrical Engineering, Technical University of Denmark, Ørsteds Plads 352, 2800 Kongens Lyngby, Denmark

(Received 11 May 2010; revised 7 September 2010; accepted 13 September 2010)

It is often enough to localize environmental sources of noise from different directions in a plane. This can be accomplished with a circular microphone array, which can be designed to have practically the same resolution over 360°. The microphones can be suspended in free space or they can be mounted on a solid cylinder. This investigation examines and compares two techniques based on such arrays, the classical delay-and-sum beamforming and an alternative method called circular harmonics beamforming. The latter is based on decomposing the sound field into a series of circular harmonics. The performance of the two signal processing techniques is examined using computer simulations, and the results are validated experimentally. © *2010 Acoustical Society of America*.
[DOI: 10.1121/1.3500669]

PACS number(s): 43.60.Fg, 43.50.Rq [EJS] Pages: 3535–3542

I. INTRODUCTION

Acoustical beamforming is a signal processing technique used to localize sound sources using microphone arrays. Unlike other array techniques such as statistically optimized near-field acoustical holography (SONAH), which are based on near-field measurements,[1,2] beamforming is based on far-field measurements, i.e., the array must be placed relatively far from the sources in order to determine their "position" by processing the signals captured by the microphones.[3]

The goal of the present work is the design of beamformers for localization of environmental noise sources. In outdoors measurements, the sound field is basically generated by sources placed far from the measurement point, in the far field. At the measurement point, the direction of propagation of the waves can be considered essentially parallel to the ground, which implies that the sound field can be assumed to be two-dimensional. For such purposes, it is suitable to use circular arrays as these are able to map the sound field over 360°.

The techniques developed for the circular geometry are delay-and-sum beamforming (DSB) and circular harmonics beamforming (CHB). The first technique is the classical beamforming technique, which is widely used since it is very robust in the presence of background noise.[4] By contrast, CHB is a novel technique that belongs to a more recent category called eigenbeamforming. All techniques in this group are based on decomposing the sound field into a summation of harmonics.[5–8] CHB has been developed by adapting the theory of spherical harmonics beamforming to the two-dimensional case using circular harmonics (CH).

II. DECOMPOSITION OF THE SOUND FIELD USING CH

A. Circular apertures

Consider a circular aperture of radius R in the xy-plane and a plane wave with amplitude P_0 that impinges on the aperture in a direction perpendicular to the z-axis in free space. The incident pressure at any point of the aperture can be written in polar coordinates,

$$p(kR,\varphi) = P_0 e^{j\mathbf{k_i}\cdot\mathbf{r}}\big|_{r=R} = P_0 e^{jkR\cos(\varphi-\varphi_i)}, \tag{1}$$

where $\mathbf{k_i}$ and φ_i are the wave number vector and the angle of the incident wave. The temporal term $e^{-j\omega t}$ has been suppressed. This expression can be expanded in series of circular waves,[9]

$$e^{jkR\cos(\varphi-\varphi_i)} = J_0(kR) + \sum_{n=1}^{\infty} 2j^n \cos(n(\varphi-\varphi_i)) J_n(kR), \tag{2}$$

where J_n is a Bessel function of order n. Developing this expression further, the pressure of the incident plane wave becomes

$$p(kR,\varphi) = P_0 \sum_{n=-\infty}^{\infty} j^n J_n(kR) e^{jn(\varphi-\varphi_i)}. \tag{3}$$

The pressure can now be represented by an infinite number of CH $e^{jn\varphi}$ (or modes) using the principle of a Fourier series. The pressure on the (unbaffled) aperture can be expressed as a function of the angle of the source φ_s using the relationship $\varphi_i = \varphi_s + \pi$,

$$p(kR,\varphi) = P_0 \sum_{n=-\infty}^{\infty} (-j)^n J_n(kR) e^{jn(\varphi-\varphi_s)}. \tag{4}$$

[a)]Portions of this work were presented in "Beamforming with a circular microphone array for localization of environmental sources of noise," Proceedings of Inter-Noise 2010, Lisbon, Portugal, June 2010.
[b)]Author to whom correspondence should be addressed. Electronic mail: etr@elektro.dtu.dk

When the same aperture is mounted on a rigid, infinite cylinder, the incident wave is scattered by the cylinder. The pressure on the baffled aperture is the superposition of the incident pressure and the scattered pressure, $p = p_i + p_s$. The scattered pressure at positions on the aperture becomes[10]

$$p_s(kR, \varphi) = \sum_{n=0}^{\infty} A_n \cos(n\varphi)(J_n(kR) + jY_n(kR)), \tag{5}$$

where the terms A_n are a set of coefficients and Y_n is a Neumann function of order n. Making use of the Hankel functions of first kind, $H_n(\cdot) = J_n(\cdot) + jY_n(\cdot)$, the previous expression can be rewritten as

$$p_s(kR, \varphi) = \sum_{n=-\infty}^{\infty} B_n H_n(kR) e^{jn\varphi}. \tag{6}$$

The terms B_n are obtained by imposing that the total velocity in the radial direction vanishes on the surface of the rigid cylinder, $u_{i,r} + u_{s,r} = 0$,

$$B_n = -P_0(-j)^n \frac{J_n'(kR)}{H_n'(kR)} e^{-jn\varphi_s}, \tag{7}$$

where J_n' and H_n' are the derivatives of the Bessel and Hankel functions with respect to the radial dimension. Using the expressions given in Eqs. (4) and (6) for the incident and the scattered wave, together with the coefficients obtained in Eq. (7), the total pressure at the surface of the rigid cylinder becomes

$$p(kR, \varphi) = P_0 \sum_{n=-\infty}^{\infty} (-j)^n \times \left(J_n(kR) - \frac{J_n'(kR) H_n(kR)}{H_n'(kR)} \right) e^{jn(\varphi - \varphi_s)}. \tag{8}$$

Comparing Eqs. (3) and (8) with a Fourier series in the exponential form[11] shows that the pressure on the baffled or the unbaffled apertures can be represented as

$$p(kR, \varphi) = \sum_{n=-\infty}^{\infty} C_n e^{jn\varphi}, \tag{9}$$

where the Fourier coefficients C_n for the two cases are

$$C_n(kR, \varphi_s) = P_0 Q_n(kR) e^{-jn\varphi_s}, \tag{10}$$

with

$$Q_n(kR) = \begin{cases} (-j)^n J_n(kR) & \text{unbaffled}, \\ (-j)^n \left(J_n(kR) - \frac{J_n'(kR) H_n(kR)}{H_n'(kR)} \right) & \text{baffled}. \end{cases} \tag{11}$$

The modulus of the first four coefficients C_n is shown in Fig. 1, for baffled and unbaffled apertures. At low values of kR, the zero order mode is constant and equals 0 dB in both cases, whereas all the other modes have a slope of $10 \times n$ dB per decade. When the aperture is baffled, the response is offset by 6 dB compared with the unbaffled case. With increasing values of kR, more and more harmonics gain strength. However, for the unbaffled aperture the response exhibits some dips that imply that signals that have components around these dips cannot be totally resolved. This problem disappears when the cylindrical baffle is used.

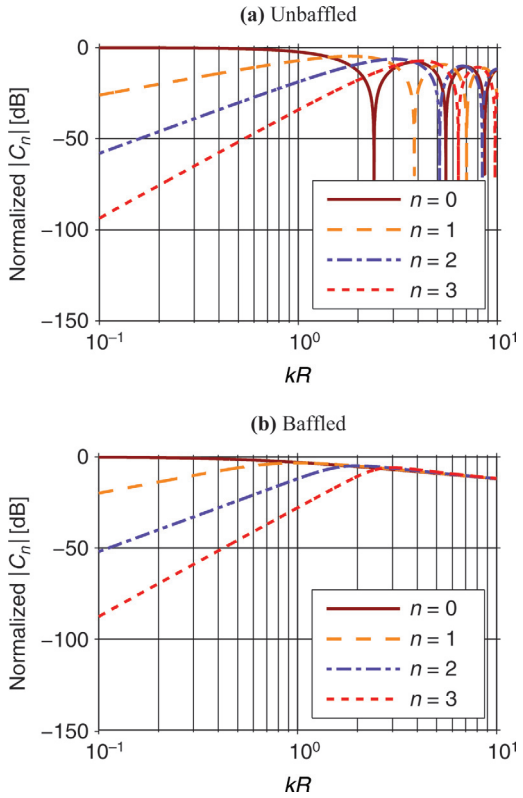

FIG. 1. (Color online) Normalized modulus of the four lowest Fourier coefficients of the pressure on an unbaffled circular aperture (top) and on a circular aperture mounted on a rigid cylindrical baffle of infinite length (bottom).

Since the curves of the Fourier coefficients are functions of kR, variation of R implies that the curves are scaled in frequency (or wave number), and vice-versa. For instance, when R is increased, the response is shifted toward low frequencies, whereas a decrease of R results in a shift toward high frequencies.

B. Implementation using microphone arrays

In principle, infinitely many Fourier terms are needed to represent the sound pressure. However, in practice the number of harmonics must be truncated to a maximum order, N. As a rule of thumb,

$$N \approx kR \tag{12}$$

is usually chosen as a first approximation.[8,12,13] The reason for this is that the amplitude of the Bessel functions in the Fourier coefficients [see Eqs. (10) and (11)] is small when the order of the Bessel functions n exceeds its argument (kR). Thus, the overall contribution of modes $|n| > kR$ is very small.

Besides, microphone arrays rather than "ideal" continuous apertures are used in real-life applications, which implies

that apertures are sampled at discrete points. Assuming that an aperture is sampled with M omnidirectional microphones placed equidistantly, the Fourier coefficients become

$$\tilde{C}_n = \frac{1}{M}\sum_{m=1}^{M} \tilde{p}(kR, \varphi_m) e^{-jn\varphi_m}, \tag{13}$$

where $\tilde{p}$ is the *measured* pressure at the mth microphone placed at an angle φ_m.

The sampling procedure introduces an error in the Fourier coefficients. For example, it can be shown that in the case of an unbaffled circular array, the Fourier coefficients resulting after the sampling are, theoretically,[12–14]

$$\begin{aligned}\tilde{C}_n(kR) = {} & P_0(-j)^n J_n(kR) e^{-jn\varphi_s} \\ & + P_0 \sum_{q=1}^{\infty} (-j)^g J_g(kR) e^{jg\varphi_s} \\ & + P_0 \sum_{q=1}^{\infty} (-j)^h J_h(kR) e^{jh\varphi_s},\end{aligned} \tag{14}$$

where $g = Mq - n$ and $h = Mq + n$. Note that the first term is identical to the Fourier coefficient of the continuous aperture; see Eq. (10), whereas the remaining terms are residuals caused by the sampling. Further examination of Eq. (14) reveals that the first term is the dominant one when $M > 2|n|$. Since the highest mode excited is N,

$$M > 2N. \tag{15}$$

In fact, inserting the approximation for N given in Eq. (12) into Eq. (15) yields the Nyquist sampling criterion:

$$M > 2kR \quad \Rightarrow \quad M > 2\frac{2\pi}{\lambda}R \quad \Rightarrow \quad \frac{\lambda}{2} > d, \tag{16}$$

where λ is the wavelength and d is the distance between two consecutive microphones. Hence, by fulfilling the relationship between M and N given in Eq. (15), the Nyquist criterion is satisfied.[14]

III. BEAMFORMING TECHNIQUES

A. CHB

The beamformer response is the output of the beamformer as a function of the steering angle, i.e., the angle at which the main beam of the beamformer is pointing. Ideally, the beamformer response should assume a maximum when the beamformer is steered toward the source at φ_s, and should be zero in all other directions; that is,

$$b_{\text{ideal}}(\varphi) = A\delta(\varphi - \varphi_s), \tag{17}$$

where A is a scale factor. This can be described in terms of a Fourier series,

$$b_{\text{ideal}}(\varphi) = \sum_{n=-\infty}^{\infty} I_n e^{jn\varphi}, \tag{18}$$

$$I_n = \frac{1}{2\pi}\int_0^{2\pi} b_{\text{ideal}}(\varphi) e^{-jn\varphi}\, d\varphi = A e^{-jn\varphi_s}. \tag{19}$$

It follows that

$$b_{\text{ideal}}(\varphi) = A\sum_{n=-\infty}^{\infty} e^{-jn\varphi_s} e^{jn\varphi}. \tag{20}$$

Using Eq. (10), the output of the ideal beamformer becomes

$$b_{\text{ideal}}(kR, \varphi) = A\sum_{n=-\infty}^{\infty} \frac{C_n(kR, \varphi_s)}{P_0 Q_n(kR)} e^{jn\varphi}. \tag{21}$$

In real implementations, the number of modes must be truncated at a reasonable value, N, and the aperture must be sampled by a number of microphones, M. Thus

$$b_{N,\text{CH}}(kR, \varphi) = A\sum_{n=-N}^{N} \frac{\tilde{C}_n(kR, \varphi_s)}{P_0 Q_n(kR)} e^{jn\varphi}. \tag{22}$$

Comparing with Eq. (10), Eq. (22) be rewritten as

$$b_{N,\text{CH}}(kR, \varphi) = A\sum_{n=-N}^{N} \frac{\tilde{C}_n(kR, \varphi_s)}{C_n(kR, \varphi)}. \tag{23}$$

When the beamformer is steered toward the position of the source, φ equals φ_s, so the quotients approximate unity and the output assumes a maximum. Note that, when using unbaffled arrays, Eq. (23) has singularities at the frequencies where the Fourier coefficients have dips; see Fig. 1. At such frequencies, the CH beamformer is not capable of resolving the location of the source properly.

Inserting the approximated coefficients given by Eq. (13) into Eq. (22), the CH beamformer output becomes

$$\begin{aligned}& b_{N,\text{CH}}(kR, \varphi) \\ & = \frac{A}{MP_0}\sum_{m=1}^{M}\left(\tilde{p}(kR, \varphi_m)\sum_{n=-N}^{N}\frac{1}{Q_n(kR)} e^{-jn(\varphi_m - \varphi)}\right).\end{aligned} \tag{24}$$

Ideally, this should be zero at all angles different from φ_s. However, since a limited number of microphones are used, the response exhibits a main lobe around φ_s and side lobes at other angles.

B. DSB

The delay-and-sum (DS) technique aligns the signals from the microphones of the array by introducing appropriate delays and finally adds them together.[3,15,16] The delays are determined by the steering direction of the array. The output assumes its maximum when the focusing direction coincides with the position of the source.

In this investigation, the output of a DS beamformer is implemented in the frequency domain using matched field

processing. This method uses phase shifts to align the signals in phase. Assuming that the beamformer is steered toward the direction φ, the beamformer output is

$$b_{\mathrm{DS}}(kR,\varphi) = A\sum_{m=1}^{M} w_m \tilde{p}(kR,\varphi_m)\cdot p^*(kR,\varphi_m,\varphi), \quad (25)$$

where

(1) w_m is the weighting coefficient of the mth microphone;
(2) $\tilde{p}(kR,\varphi_m)$ is the pressure measured at the mth microphone position due to a plane wave generated by a source at φ_s; and
(3) $p^*(kR,\varphi_m,\varphi)$ is the *theoretical* complex conjugated pressure that would be captured at the mth microphone due to plane wave generated at φ. Note that the argument φ is used to emphasize that this is the variable that defines the focusing direction of the beamformer.

In general, the source position is unknown, and therefore the beamformer must map over all possible source positions, i.e., $0 \le \varphi < 2\pi$. The key point is that when the beamformer is focused toward the position of the source φ_s, the second and the third terms of Eq. (25) become equal in magnitude but opposite in phase. In these circumstances, the microphone signals are aligned in time, and therefore the maximum output of the beamformer is reached.

In the case of an unbaffled array, the theoretical pressure is simply the closed form for a plane wave, so the beamformer output is

$$b_{\mathrm{DS}}(kR,\varphi) = A\sum_{m=1}^{M} w_m \tilde{p}(kR,\varphi_m) P_0 e^{-j\mathbf{k}_i\cdot\mathbf{r}}\Big|_{r=R} = \frac{AP_0}{M}\sum_{m=1}^{M}\tilde{p}(kR,\varphi_m)e^{jkR\cos(\varphi_m-\varphi)}. \quad (26)$$

Since all microphones have equal "importance," the weights w_m have been set to $1/M$. For the baffled array, the output of the beamformer is obtained by introducing Eq. (9) into Eq. (25), and taking into account that the number of modes used for the processing is truncated at a number N,

$$b_{N,\mathrm{DS}}(kR,\varphi) = \frac{AP_0}{M}\sum_{m=1}^{M}\left(\tilde{p}(kR,\varphi_m)\sum_{n=-N}^{N} Q_n^*(kR)e^{-jn(\varphi_m-\varphi)}\right). \quad (27)$$

This expression is also valid for the unbaffled case, although it is not as precise as Eq. (26) because of the truncation.

Further analysis of Eq. (27) reveals that the beamformer output can be written, according to Eqs. (10) and (13), as

$$b_{N,\mathrm{DS}}(kR,\varphi) = A\sum_{n=-N}^{N}\tilde{C}_n(kR,\varphi_s)\cdot C_n^*(kR,\varphi). \quad (28)$$

As opposed to CHB, where the beamformer output could be expressed as the ratio of the approximated coefficients to the theoretical ones [see Eq. (23)], the output of the DS beamformer is a multiplication of these terms. Therefore, in the case of unbaffled arrays, the singularities that can be present in CHB because of the dips of the Fourier coefficients are totally resolved with a DS beamformer.

C. Beamformer performance—Resolution and maximum side lobe level (MSL)

The resolution of a beamformer is defined as the −3 dB width of the main lobe of the beampattern. This parameter is of interest because it gives an approximation to the minimum angular difference between two incoherent sources that is necessary in order to distinguish them from each other.

The beamformer output will usually exhibit side lobes. This is an unwanted effect as the beamformer seems to be sensitive not only in the focusing direction but also in the direction of the side lobes. Therefore, it is convenient to evaluate the beamformer response by means of the MSL. This parameter is the difference in level between the peak of the highest side lobe and the peak of the main lobe.

IV. SIMULATIONS

The performance of circular arrays with CHB and DSB has been evaluated by means of simulations. The circular arrays have radii of 10 and 20 cm and 10 and 20 microphones, respectively. The number of microphones and the radius of each array were chosen by setting the same maximum frequency that could be represented without any sampling error (around 2.7 kHz); see Sec. II B. The simulations were carried out under ideal conditions, i.e., without background noise. The source was placed at 180°, but the source position has a very limited influence on the results. The amplitude of the waves impinging on the array was the same at all frequencies.

A. Simulations with CHB

The resolution and the MSL obtained with CHB and an unbaffled circular array are shown in Fig. 2, for the range from 50 Hz to 3.5 kHz. The number of orders used in the CHB algorithm given in Eq. (24) followed $N = \lceil kR \rceil$, where $\lceil\cdot\rceil$ is the ceiling function. The maximum value of N was $M/2 - 1$ in order to fulfill Eq. (15).

As can be seen, the resolution and the MSL are constant for a certain interval. This depends on the number of orders N used for the processing. The fact that the main lobe becomes narrower from interval to interval indicates an improvement in the resolution. More intervals, i.e., more orders, result in a better resolution, which is the case of the array of largest radius. The MSL follows the same behavior as the resolution, improving when the number of orders is increased. The staircase pattern in these two measures is also obtained with spherical harmonics beamforming.

At some frequencies an "unexpected" response occurs, e.g., around 2.1 kHz for the array of 10 cm and 2.8 kHz for the array of 20 cm. This phenomenon is due to the dips in the Fourier coefficients obtained with unbaffled arrays. The frequencies where this phenomenon occurs cannot be resolved as precisely as the neighboring frequencies. This

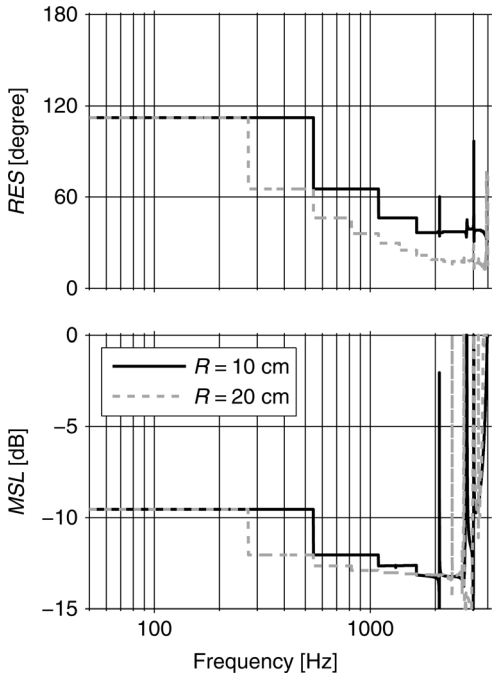

FIG. 2. Resolution and MSL using CHB and unbaffled arrays of radii 10 and 20 cm and 10 and 20 microphones, respectively. The source is placed at 180°.

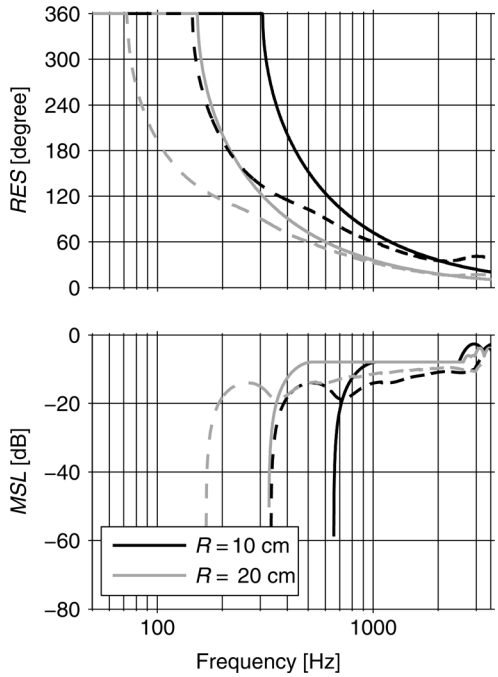

FIG. 3. Resolution and MSL using DSB and circular arrays of radius 10 and 20 cm and 10 and 20 microphones, respectively. Solid lines: Unbaffled arrays; dashed lines: Baffled arrays. The source is placed at 180°.

effect is avoided when the array is mounted on a rigid cylindrical baffle. The overall behavior of the CH beamformers when baffled arrays are used is very similar to the unbaffled case but without the problem of unresolved frequencies.

The arrays can be used up to a maximum frequency without any sampling error. For the arrays under analysis, this occurs at about 2.7 kHz. Above this frequency, the effect of the sampling error can be seen especially in the MSL (the magnitude of the side lobes is higher than in the previous interval of frequencies).

B. Simulations with DSB

The resolution and the MSL obtained under ideal conditions using DSB are shown in Fig. 3 for both baffled and unbaffled arrays. In the case of baffled arrays, the number of orders used in the DSB algorithm, stated in Eq. (27), was $N = \lceil kR \rceil + 1$, up to a maximum $N = M/2 - 1$ according to Eq. (15).

It is apparent that the resolution is 360° at low frequencies in all cases, and the MSL is non-existent, meaning that the beamformer is omnidirectional. From a certain frequency depending on the radius of the array, the resolution improves continuously until high frequencies. The curves decay in a similar way for both kinds of arrays, but in the baffled case they exhibit small smooth fluctuations. The MSL curves begin at a certain frequency and grow progressively until a maximum level is reached. In the case of unbaffled arrays, this level remains constant, whereas for baffled arrays the MSL exhibits ripples while it increases toward high frequencies. Nevertheless, the MSL is better for baffled arrays than for unbaffled.

In both cases, the performance improves with increasing radius of the array and is better in the case of baffled arrays. Furthermore, it can be seen that the baffled array of 10 cm of radius has resolution and MSL similar to the unbaffled array of radius 20 cm. Thus it can be concluded that mounting an array on an infinite baffle makes it seem to be "larger" than in the unbaffled case. Similar characteristics are found when DSB is applied to spherical arrays.

In general the resolution obtained with DSB is much worse than the resolution obtained with CHB. At high frequencies, the MSL with DSB is worse than with CHB for unbaffled arrays; but the opposite is the case for baffled arrays.

V. EXPERIMENTAL RESULTS

A prototype array with a radius of 11.9 cm has been tested in an anechoic room with a volume of about 1000 m^3. The array was constructed by mounting twelve 1/4 in. microphones, Brüel & Kjær (B&K) Type 4935, on a circular frame, corresponding to a microphone for every 30°. The implemented prototype is shown in Fig. 4.

The array and the source, a loudspeaker, were controlled by a B&K PULSE Analyzer. In all the measurements the loudspeaker was driven by a signal from the generator, pseudorandom noise of 1 s of period, 3.2 kHz of bandwidth, and 1 Hz of resolution. The microphones signals were recorded with the analyzer and postprocessed with the beamforming algorithms DSB and CHB.

The normalized outputs obtained with both CHB and DSB are shown on top of Fig. 5, whereas the simulated outputs are provided in the bottom. To account for the background noise introduced in the measurements, the simulations were carried out with a signal-to-noise ratio (SNR) of 30 dB at the input of each microphone due to uniformly distributed noise.

FIG. 4. (Color online) Circular array with radius of 11.9 cm and 12 microphones. Prototype by Brüel & Kjær.

The results agree very well with the theoretical ones for both techniques. A few differences deserve to be mentioned in the case of CHB. The side lobes are somewhat deformed and blurred compared with the simulations. The output is not only distorted at the frequencies that coincide with the dips in the Fourier coefficients, but also at frequencies in their vicinity. This phenomenon is particularly pronounced around 1.7 kHz. These differences are suspected to be caused by the CH beamformer algorithm itself, because of the fact that the approximated Fourier coefficients are compared with the theoretical ones in a ratio. When the approximate coefficients match the theoretical ones, the beamformer output is similar to the pattern expected under ideal conditions.

The agreement between measurements and simulations can be further examined by studying the resolution and the MSL. These quantities are shown in Fig. 6. The resolution using CHB is very similar to the one obtained with the simulation. The response follows the simulation curve rather accurately even at the frequencies where singularities occur. Some small deviations can be observed at the lowest frequencies, which are attributed to the influence of background noise. In contrast to the resolution, the MSL deviates somewhat from the simulation. In general, this measure is slightly higher than the expected one and worsens near singularities. At frequencies below 100 Hz a significant influence of background noise in the measurement becomes apparent.

For DSB, there are only a few differences compared with the simulations. The first is that the resolution equals 360° up to a frequency 20 Hz higher than expected. The second difference is that the first side lobe appears at 634 Hz instead of 556 Hz as obtained in the simulation. Yet another difference is that MSL is better than expected in the range from 1950 Hz to about 2300 Hz. These differences are again mainly attributed to the differences between the measured pressure and the theoretical one. However, the beampattern as well as the resolution and the MSL are not as much affected by these differences as in the case of CHB. This characteristic

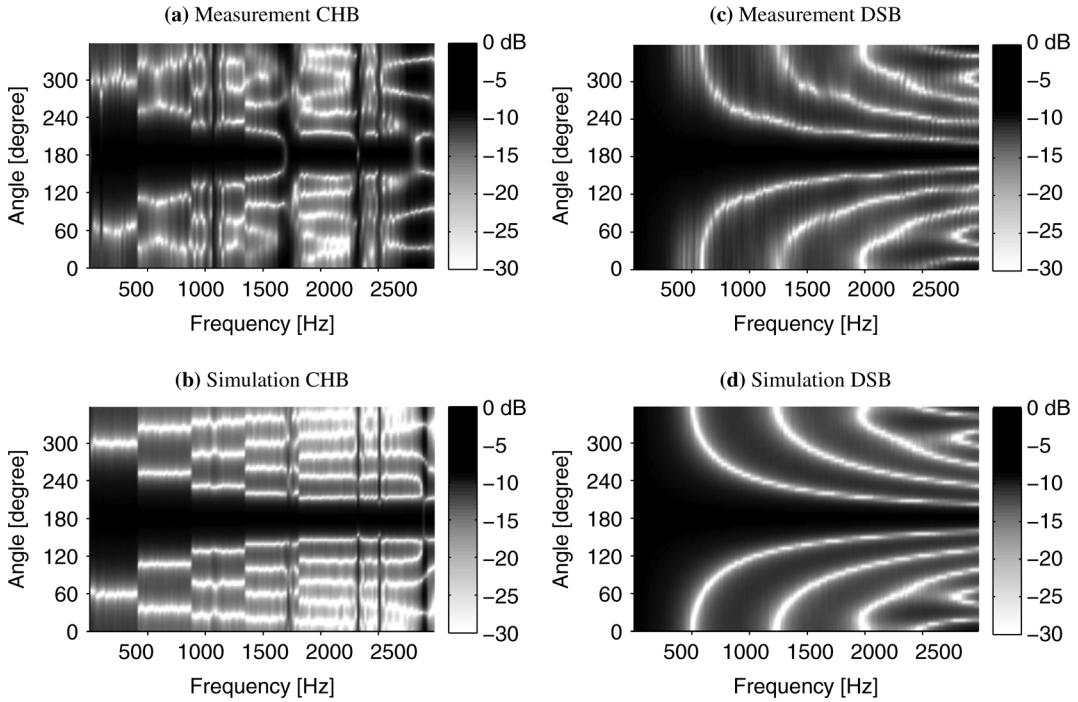

FIG. 5. Normalized output using CHB [(a), (b)] and DSB [(c), (d)] and an unbaffled array with a radius of 11.9 cm with 12 microphones. The source is placed at 180°. The top panels (a) and (c) show the measurements performed with a prototype, whereas the corresponding simulation is presented in the bottom panels (b) and (d). For the simulation, an SNR of 30 dB in each microphone is considered.

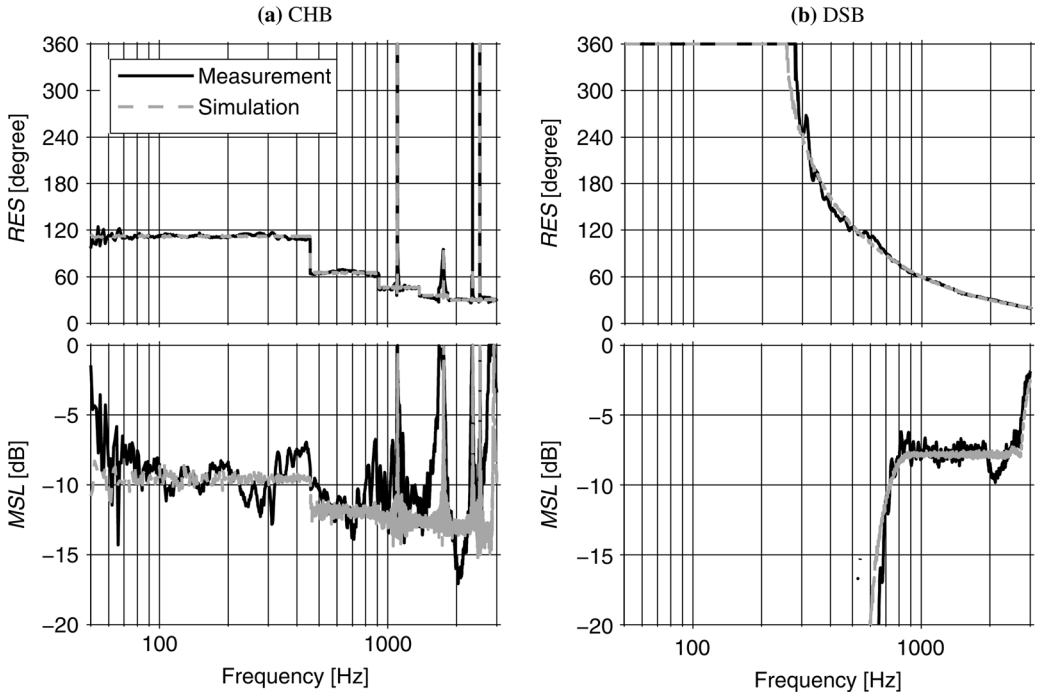

FIG. 6. Resolution and MSL using CHB (left) and DSB (right) and an unbaffled array with a radius of 11.9 cm with 12 microphones. The source is placed at 180°. The theoretical case obtained by simulation is also shown. The SNR in each microphone is set to 30 dB for the simulation.

and the fact that the influence of background noise is lower than CHB demonstrate that DSB is a more robust algorithm.

VI. CONCLUSIONS

Two different beamforming techniques based on circular arrays have been examined theoretically and experimentally, CHB and the well-known DSB. CHB is an adaptation of the spherical harmonics beamforming technique to a circular geometry.

The prototype used for the experimental investigation gave very satisfactory results: The beampatterns, the resolution, and the MSL were found to be in extremely good agreement with simulations for both CHB and DSB.

For a given array, CHB has better resolution and lower MSL in a wider frequency range than DSB has. Regardless of the technique, these quantities improve with increasing frequency. The frequency range is limited at low frequencies by the influence of background noise in the case of CHB and by the fact that the output becomes omnidirectional for DSB. At high frequencies, the limitation is in both cases given by the increase of the sampling error.

Keeping the number of microphones constant, the beamformer response is scaled in frequency when the radius of the array is modified. However, when the radius of the array is kept constant but the number of microphones is increased, the response improves toward higher frequencies since the spacing between the microphones becomes smaller. In fact, by increasing the number of microphones, the array behaves more similarly to a continuous aperture.

A given ratio between the number of microphones and the radius of the array determines the upper frequency above which a sampling error occurs. In such case, the overall performance improves considerably toward lower frequencies when increasing the radius. However, the number of microphones should be increased accordingly, otherwise the upper limit frequency would be reduced.

In the presence of background noise, DSB is more robust than CHB, and CH beamformers exhibit singularities, i.e., frequencies that cannot properly be resolved, when unbaffled circular arrays are used. This problem would be solved if it were feasible to mount the arrays on rigid cylindrical baffles of infinite length. The performance of DS beamformers would also improve substantially by mounting the arrays on rigid cylindrical baffles of infinite length, but this is not realistic.

CHB can be used in the entire frequency range except at the frequencies that cannot be properly resolved due to the nature of this technique. At such frequencies, it is convenient to use DSB instead. In addition to this, DSB should not be underestimated in environments with a poor SNR because of its robustness.

ACKNOWLEDGMENTS

The authors would like to thank Karim Haddad and Jørgen Hald, Brüel & Kjær, for lending us a circular microphone array and other equipment for the beamforming measurements. We would also like to thank Julien Jourdan and Marton Marschall for their notes about spherical harmonics beamforming, which became very helpful for the present work.

[1]J. Maynard, E. Williams, and Y. Lee, "Nearfield acoustic holography: I. Theory of generalized holography and the development of NAH," J. Acoust. Soc. Am. **78**(4), 1397–1413 (1985).
[2]J. Hald, "Basic theory and properties of statistically optimized near-field acoustical holography," J. Acoust. Soc. Am. **125**(4), 2105–2120 (2009).
[3]J. Hald, "Beamforming and wavenumber processing," in *Handbook of Signal Processing in Acoustics*, edited by D. Havelock, S. Kuwano, and M. Vorländer (Springer, New York, 2008), Chap. 9, pp. 131–144.

[4]J. Bitzer and K. Uwe Simmer, "Superdirective microphone arrays," in *Microphone Arrays. Signal Processing Techniques and Applications*, edited by M. Brandstein and D. Ward (Springer, Berlin, 2001), Chap. 2, p. 26.
[5]B. Rafaely, "Plane-wave decomposition of the sound field on a sphere by spherical convolution," J. Acoust. Soc. Am. **116**(4), 2149–2157 (2004).
[6]W. Song, W. Ellermeier, and J. Hald, "Using beamforming and binaural synthesis for the psychoacoustical evaluation of target sources in noise," J. Acoust. Soc. Am. **123**(2), 910–924 (2008).
[7]H. Teutsch and W. Kellermann, "Acoustic source detection and localization based on wavefield decomposition using circular microphone arrays," J. Acoust. Soc. Am. **120**(5), 2724–2736 (2006).
[8]H. Teutsch, *Modal Array Signal Processing: Principles and Applications of Acoustic Wavefield Decomposition* (Springer, Berlin, 2007), pp. 150–188.
[9]P. Morse and H. Feshbach, *Methods of Theoretical Physics* (McGraw-Hill, New York, 1953), Vol. I, p. 828.
[10]P. Morse, *Vibration and Sound*, 2nd ed. (McGraw-Hill, New York, 1948), pp. 347–348.
[11]E. Williams, *Fourier Acoustics: Sound Radiation and Nearfield Acoustic Holography* (Academic Press, London, 1999), pp. 4–5.
[12]C. Mathews and M. Zoltowski, "Eigenstructure techniques for 2-D angle estimation with uniform circular arrays," IEEE Trans. Signal Process. **42**(9), 2395–2407 (1994).
[13]D. E. N. Davies, "Circular arrays," in *The Handbook of Antenna Design*, edited by A. W. Rudge, K. Milne, A. D. Olver, and P. Knight (Peter Peregrinus Ltd., London, 1983), Vol. II, Chap. 12, pp. 298–310.
[14]H. Van Trees, *Optimum Array Processing. Part IV of Detection, Estimation, and Modulation Theory* (Wiley, New York, 2002), pp. 280–284.
[15]D. Johnson and D. Dudgeon, *Array Signal Processing Concepts and Techniques* (Prentice Hall, Englewood Cliffs, NJ, 1993), pp. 112–119.
[16]G. Elko and J. Meyer, "Microphone arrays," in *Springer Handbook of Speech Processing*, edited by J. Benesty, M. Sondhi, and Y. Huang (Springer-Verlag, Berlin, 2008), Chap. 50, pp. 1021–1042.